Chinese Chemical Letters 35 (2024) 108710

Contents lists available at ScienceDirect

Chinese Chemical Letters

journal homepage: www.elsevier.com/locate/cclet

Functional nanoemulsions: Controllable low-energy nanoemulsification and advanced biomedical application

Maojie Zhang[a], Qiang Cao[b], Yuming Yuan[a], Xiaohan Guo[a], Dawei Pan[b,c], Rui Xie[b,c], Xiaojie Ju[b,c], Zhuang Liu[b,c], Wei Wang[b,c,*], Liangyin Chu[b,c]

[a] College of Engineering, Sichuan Normal University, Chengdu 610101, China
[b] School of Chemical Engineering, Sichuan University, Chengdu 610065, China
[c] State Key Laboratory of Polymer Materials Engineering, Sichuan University, Chengdu 610065, China

ARTICLE INFO

Article history:
Received 23 March 2023
Revised 14 June 2023
Accepted 19 June 2023
Available online 22 June 2023

Keywords:
Nanoemulsions
Interfaces
Drug delivery
Template synthesis
Nanoparticles

ABSTRACT

Nanoemulsions are widely used as advanced pharmaceutical delivery systems in biomedical field, due to their high encapsulation efficiency and good therapy efficacy. Nanoemulsification techniques that produce nanoemulsions with controllable sizes and compositions are promising for creating advanced nanoemulsion systems for pharmaceutical delivery. This review summarizes recent advances on low-energy emulsification techniques for producing nanoemulsions, and the use of these nanoemulsions as advanced pharmaceutical delivery systems and as templates to create drug-loaded functional particles for biomedical application. First, nanoemulsification techniques that utilize elaborate interfacial physics/chemistry and micro-/nano-fluidics, featured with relatively-low energy input, to produce nanoemulsions with controllable sizes and compositions, are introduced. Uses of these nanoemulsions to create nanoemulsion-incorporated milli-particles, drug-loaded nanoparticles and nanoparticle-incorporated microparticles with sizes ranging from several millimeters to sub-10 nm are emphasized. Flexible and efficient use of the nanoemulsions, functional nanoparticles and milli-/micro-particles integrated with nanoemulsions or nanoparticles for advanced pharmaceutical delivery in biomedical field are highlighted, with focus on how the interplay between their sizes and compositions achieve desired pharmaceutical-delivery performances. Finally, perspectives on further advances on the controllable production of nanoemulsions are provided.

1. Introduction

Nanoemulsions (NEs) are heterogeneous systems consisting of immiscible liquid phases (usually oil and water), with surfactant-stabilized nanodroplets of one liquid dispersed in the other continuous one. Due to the small size, NEs show features of good transparency, high surface area, robust stability, and tunable rheology, thus finding diverse applications in fields such as biomedical science, food, cosmetics, and material synthesis [1–9]. In biomedical filed, NEs are widely used as advanced delivery systems for active ingredients such as therapeutic and diagnostic agents, due to their features such as low toxicity, high encapsulation efficiency, improved thermodynamic stability, and good biodegradability and biocompatibility [10,11]. Typically, the nano-size of NEs enables precise pharmaceutical delivery to specific tissues and organs, due to the size-dependent biodistribution in biological systems [12], while their high surface area further benefits greater absorption and higher bioavailability [13,14]. The tunable composition of oil and water phases in NEs enables flexible loading of hydrophobic and hydrophilic ingredients, while the tailorable surface property of nanodroplets benefits their interaction with the cells to achieve improved efficacy. Moreover, with deformable fluidic nature and nanoscale size, NEs can be manipulated into versatile dosage forms such as liquids, creams, gels, and foams, and flexibly administrated *via* routes such as oral, transdermal, ocular, and nasal routes [13,14]. Thus, with tailored sizes and compositions, NEs can achieve remarkable physicochemical and biopharmaceutical features for advanced pharmaceutical delivery applications.

Generally, NEs are formed by mixing oil and water phases with the assistance of surfactant molecules. The nanoemulsion systems generally include O/W NEs (with oil nanodroplets dispersed in water) and W/O NEs (with water nanodroplets dispersed in oil). During the emulsification process, the dispersed phase is deformed

* Corresponding author at: School of Chemical Engineering, Sichuan University, Chengdu 610065, China.
E-mail address: wangwei512@scu.edu.cn (W. Wang).

https://doi.org/10.1016/j.cclet.2023.108710
1001-8417/

and broken up into nanoscale droplets, associated with huge interface expansion, as well as significantly increased interfacial energy [15]. The amphiphilic surfactant molecules play a key role in this emulsification process, due to their capability to stabilize the interfaces of the heterogeneous nanoemulsion system. The amphiphilic surfactants with their hydrophilic group into water phase and hydrophobic group into the oil phase, can lower the interfacial tension between the oil and water phases, and provide a physical interfacial barrier for droplet stabilization. However, although the surfactants lower the interfacial tension and energy barrier for forming the highly curved surface of nanodroplets, emulsification of a biphasic liquid mixture into a large quantity of nanodroplets is still associated with huge expansion of the liquid-liquid interfaces. Thus, such a nanoemulsification process requires energy input to overcome the significant interfacial energy barrier for the huge interface expansion [16]. Usually, the required energy for interfacial impact can be offered by external energy input (*e.g.,* mechanical energy), internal energy (*e.g.,* physicochemical energy) of the liquid mixtures, or combination of both [15,17,18]. Nanoemulsification techniques that can form NEs with controllable sizes and compositions are promising for creating advanced NEs systems for pharmaceutical delivery applications.

This review summarizes recent advances on low-energy nanoemulsification techniques for creating NEs, and the use of these NEs as advanced pharmaceutical delivery systems and as templates to create drug-loaded functional polymeric particles for biomedical application. First, nanoemulsification techniques with relatively-low energy input, that utilize elaborate interfacial physics/chemistry and micro-/nano-fluidics to produce NEs with controllable sizes and compositions, are introduced. Use of the NEs as templates to create drug-loaded nanoparticles (NPs) with sizes ranging from several hundreds of nanometers to sub-10 nanometers, and NEs-incorporated or NPs-incorporated particles are emphasized. Then, flexible and efficient uses of the NEs, functional NPs and NEs-incorporated or NPs-incorporated particles, for advanced pharmaceutical delivery in biomedical field are highlighted. How the interplay between the sizes and compositions of delivery systems, including the NEs, NPs and composite particles realize desired advanced pharmaceutical delivery performances for biomedical application is discussed. Finally, perspectives on future study for controllable production of NEs are provided. This review provides guidelines with interfacial physics/chemistry insights for rational design and production of desired NEs and NEs-derived particles for pharmaceutical delivery.

2. Formation of nanoemulsions

Generally, nanoemulsification techniques for creating NEs can be typically classified into the high-energy methods and low-energy methods [14,15,17]. The high-energy methods usually harness the mechanical energy from processes such as ultrasonication, high-pressure homogenization and high-shear mixing to impart high shear stress on liquid phases for interface expansion [15,18]. These methods usually produce nanoscale emulsion droplets with polydisperse sizes. Moreover, these methods show low energy efficiency, since most (∼99%) of the input energy is lost as heat dissipation due to friction [19]. In low-energy methods, the nanoemulsion production mainly utilizes the internal physicochemical energy of the non-equilibrium liquid system, rather than the mechanical energy from external dispersion equipment [15,17]. Such a non-equilibrium state of liquid mixtures can be achieved by adjusting the composition (changing surfactant concentration, or dilution) [20] or temperature [21,22]. Practical use of such low-energy nanoemulsification usually employs the combination of both external energy and internal chemical energy of the system for nanoemulsion production. As compared to the high-energy methods, the low-energy methods usually produce nanoemulsion droplets with more uniform sizes. Such NEs can provide more predictable properties, and thus are preferred for uses in fields such as biomedical and catalytic fields. Since the high-energy methods and phase inversion methods are well reviewed by literatures [6,15], here we mainly focus on recent advances of nanoemulsification methods, including those require relatively-low energy input and utilize microfluidics, to offer more flexible nanoemulsification choices.

2.1. Vapor condensation method

Organic phase enriched with amphiphilic molecules allows capture of water molecules from water [23–25], and its vapor [26,27], to produce nanodroplets as templates for creating nanoscale pores in particles and membranes. When a subcooled surfactant-rich oil bath is used, it allows spontaneous condensation of water vapor into the oil phase to produce W/O NEs (Fig. 1a) [28]. Besides used for interfacial stabilization of the water nanodroplets, the surfactants in the vapor condensation method control the spreading dynamics of oil on the nucleated water at the oil/air interface to produce water nanodroplets. In a typical vapor condensation process, a cooled oil bath is placed in a chamber with high relative humidity of 75%–80% and temperature of 20 °C (Fig. 1a). The oil bath contains dodecane with low vapor pressure and low water solubility, and oil-soluble surfactant Span 80. With the temperature of oil cooled down to 2 °C, lower than the dew point (13 ± 1 °C) of air, vapor condensation occurs at the oil/air interface to form water droplets *via* heterogeneous nucleation. Due to the proper combination of interfacial tensions among the air, water and Span-80-containing dodecane, this system ensures a positive spreading coefficient to allow the oil phase spontaneously spreading over the condensed water phase for formation of water nanodroplets cloaked by a thin oil film. Since the spreading time is on the order of 10^{-12} s to 10^{-9} s, the droplet growth at the air/oil interface is largely suppressed to benefit the formation of nanoscale emulsion droplets [29]. Thus, for such a system, W/O NEs with peak radius of ∼100 nm and polydispersity of ∼10% can be produced (Fig. 1b). During the vapor condensation process, the surfactant concentration and condensation time play key roles in determining the size and polydispersity of the formed droplets. For such a method, it requires high concentration of the surfactant in the oil, at least ten times its critical micelle concentration (C_{CMC}) for production of nanoemulsion droplets. With concentration of Span 80 (0.1 mmol/L) lower than the critical surfactant concentration for cloaking condensed water, water droplets with sizes of several micrometers are formed. With the Span 80 concentration increasing to 100 mmol/L, higher than the critical surfactant concentration, water nanodroplets with sizes of several hundreds of nanometers can be produced. Moreover, with the condensation time increasing from 2 min to 30 min, the water nanodroplets formed in dodecane with 100 mmol/L Span 80 show a slightly increased peak radius and wider size distributions (Fig. 1b) [28].

The vapor condensation strategy can also be used for liquid systems with NPs as interfacial stabilizers [30]. The NPs can adsorb at the O/W interface and serve as rigid barriers to stabilize the interface [31,32]. When condensation of water vapor in a cooled kerosene bath, droplet nuclei are formed at the oil/air interface, and then engulfed by the spreading of kerosene (Fig. 1c) [30]. The droplets in the oil phase then grow to larger ones *via* coalescence until they are effectively covered by silica NPs. In this W/O system, the NPs can irreversibly adsorb at the W/O interface due to their much higher desorption Gibbs free energy than their thermal energy [31]; thus, the competition between the adsorption kinetics of NPs and growth dynamics of nanodroplets determines the droplet size. Typically, with silica NPs dispersed in

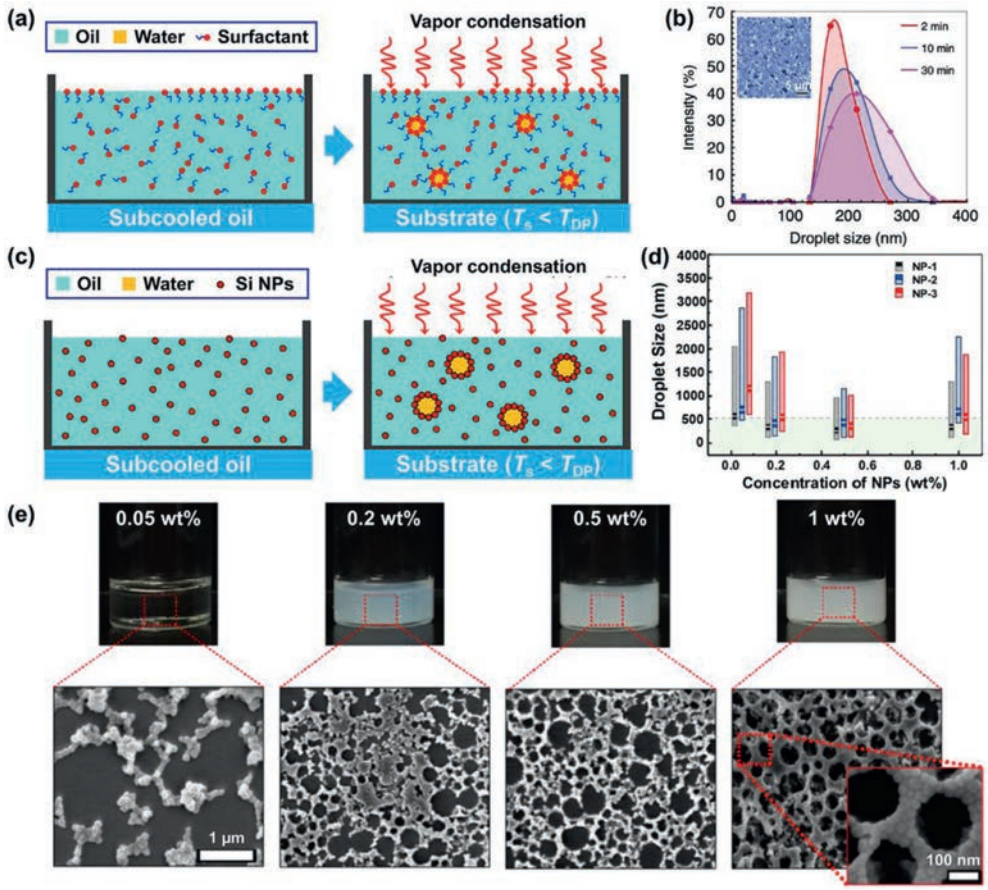

Fig. 1. Production of NEs *via* vapor condensation. (a) Illustration of condensation of vapor with high humidity into a cooled oil bath containing surfactants to produce W/O NEs. (b) Condensation-time dependent change of size distribution for water nanodroplets formed by condensing vapor into dodecane with 100 mmol/L Span 80. Reproduced with permission [28]. Copyright 2017, Springer Nature. (c) Illustration of condensation of vapor with high humidity into a cooled oil bath containing NPs to produce W/O Pickering NEs. (d) Size distribution of Pickering NEs stabilized by silica NPs with sizes of 13 ± 2.1 nm (NP-1), 52 ± 4.1 nm (NP-2) and 92 ± 10.3 nm (NP-3), and with different concentrations. (e) Photographs and SEM images of Pickering NEs stabilized by different contents of NP-2. Reproduced with permission [30]. Copyright 2018, American Chemical Society.

the kerosene bath, highly monodisperse Pickering NEs with sizes of 100∼500 nm can be formed *via* the vapor condensation process. Similarly, the size of water nanodroplets can be well controlled by adjusting the size and concentration of silica NPs, and the condensation time. As demonstrated in Fig. 1d, the size and polydispersity of the water nanodroplets show decreased values with concentration of silica NPs increasing from 0.05 wt% to 0.5 wt%. With a low concentration (0.05 wt%), the silica NPs cannot efficiently cover the condensed water nanodroplets, thus leading to coalesced droplets in micrometer sizes precipitated at the bottom of the container (Fig. 1e). Increasing the concentration of silica NPs to 0.2 wt%, 0.5 wt%, and 1 wt% allows production of water droplets with nanometer sizes (Fig. 1e). Such a vapor condensation method provides a simple scalable process for nanoemulsion production.

2.2. Cycled cooling-heating method

The cycled cooling-heating method harnesses narrow-range temperature cycling for spontaneous and repeated bursting of the dispersed droplets into numerous smaller daughter nanodroplets during the cycled freezing and melting process (Figs. 2a and b) [21,33]. During the cooling-heating process, the initial droplets are cooled to achieve the breakup or freezing, and then heated back for one cycle, with the aqueous medium kept at the liquid state. The energy of phase transition harnessed during the cooling and freezing is transformed into the large interfacial energy of the final nanodroplets. Such droplet breakup process involves three mechanisms (Fig. 2a). The first mechanism involves breakup of droplets spontaneously during cooling with platelet puncture and bursting, while the second and third mechanisms respectively involve bursting of frozen particles on melting with capillary instability of long fibres and melt-crystal fragmentation [21].

This method without external mechanical energy input provides an efficient and scalable process for nanoemulsification at low concentrations of surfactant (*ca.* 0.1-3 wt%). Such a process is applicable for various oil-surfactant combinations, such as the O/W emulsions of linear alkanes with chain length varying from C_{14} (tetradecane) to C_{20} (eicosane). As shown in Fig. 2c, for these alkane-in-water emulsions with initial droplet size of 35 μm, their median number diameter reduces to lower than 1 μm for all C_{14} to C_{17} alkanes after the first cooling-heating cycle, while their mean volume–surface diameter rapidly reduces with each cycle for all C_{15} to C_{19} alkanes.

With such a cycled cooling-heating method, initial droplets with sizes of 6 μm in batch emulsions can be converted into smaller droplets with sizes of 1.1 ± 0.2 μm after the first cooling-heating cycle. Then, in the subsequent cooling-heating cycles, the droplet size further reduces to the nanometer range (600 ± 100 nm) (Fig. 2d). Moreover, these NEs can achieve a polydispersity in the range of 1.2-1.4 (Fig. 2e). This method is efficient for larger emulsion volumes and fractions, and can be used in a continuous operational mode by flowing the emulsions along repeated pairs of conventional heating and cooling chambers.

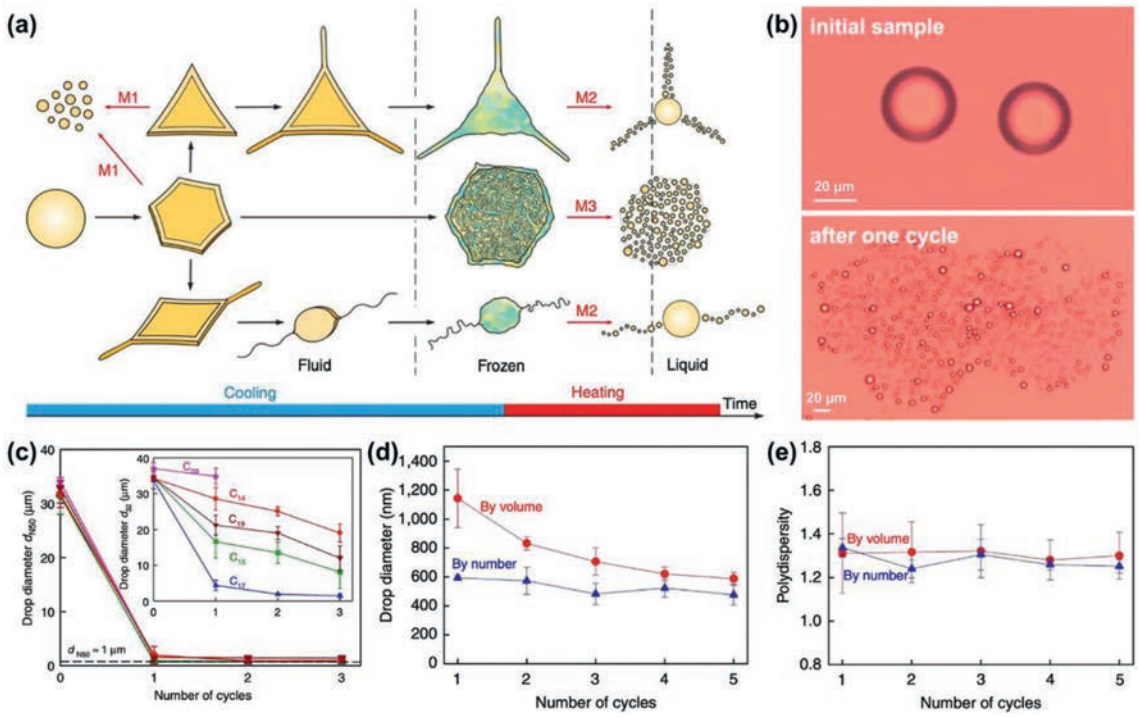

Fig. 2. Production of NEs *via* cycled cooling-heating process. (a) Illustration of the transformation of droplets and the related three mechanisms for droplet fragmentation (M1∼M3) during cooling and heating of dispersed alkane droplets. (b) Micrographs of the initial droplets of pentadecane emulsion stabilized by 1.5 wt% surfactant $C_{16}SorbEO_{20}$, and the generated daughter droplets after a cooling/heating cycle. (c) Changes of the median number diameter, and the mean volume–surface diameter (inset) during the cooling-heating cycles for alkane-in-water emulsions stabilized by $C_{18}EO_{20}$. Droplet size (d) and polydispersity (e) by volume and by number for self-emulsification in bulk emulsions with initial mean volume-surface diameter of 6 μm. Reproduced with permission [21]. Copyright 2017, Springer Nature.

2.3. Self-division method

Packing of surfactant molecules at interface is important for stabilizing the interface of droplets. Interestingly, with a chemical reaction to quickly create overpopulated surfactant molecules at the O/W interface, hydrodynamic interfacial instability can be induced to achieve interface deformation, due to the largely reduced interfacial tension [34,35]. With the chemical reaction to continuously create surfactants, the interface deformation can lead to cycles of droplet elongation and division to produce smaller and smaller progeny droplets [34,36,37].

Typically, for droplets of dichloromethane (DCM) and 2-hexyldecanoic acid (2-HDA) in an aqueous KOH solution with pH 12, NEs with sizes of ∼30 nm can be produced *via* self-division upon the interfacial reaction (Figs. 3a and b) [34]. When contacting with KOH at the O/W interface, the 2-HDA molecules are deprotonated to achieve interfacial stabilization ability like surfactants. During the neutralization reaction at the O/W interface, deprotonated 2-HDA molecules accumulate at the O/W interface, which tends to expand the interfacial area. Since the O/W interfaces during chemical reaction become unstable [37], the mother droplet spontaneously elongates and divides into several smaller daughter droplets due to Plateau-Rayleigh instability. The daughter droplets then undergo repeated self-division process to produce nanoemulsion droplets. Since the deprotonation of 2-HDA is highly pH-dependent, change of pH in the KOH solution allows manipulation of the interfacial property of the 2-HAD-laden interface, as well as the resultant nanodroplet size. In such cases, no division occurs for DCM/2-HDA microdroplets at pH lower than 10. With pH ≥ ∼10, the microdroplets undergo self-division process to produce nanodroplets with sizes of ∼30 nm. The resultant NEs are thermodynamically stable due to the electrostatic repulsions between the deprotonated 2-HDA molecules at the droplet interfaces. Decreasing pH to lower than the pK_a of 2-HAD leads to metastable coalesced droplets with increased size due to the reduced electrostatic repulsions.

Such a self-division process allows evenly partitioning nanomaterials in the microscopic mother droplet into the resultant nanodroplets [34]. This can be typically observed for water droplets containing metal nanorods (NRs) with length of 41 ± 4.2 nm and diameter of 10.5 ± 1.1 nm, in KOH solution. These nanorods are stabilized by mercaptoundecanoic acid and poly(vinyl pyrrolidone) to ensure their well distribution in the water droplets and even partition into the progeny nanodroplets. During the interfacial reaction in KOH solution with pH 12, the macroscopic water droplets with the nanorods spontaneously divide into nanodroplets (350 ± 30 nm), each encapsulating several NRs (Figs. 3c and d). The self-division method induced by chemical reaction is usually applicable to emulsion systems with immiscible or poorly-miscible oil/water phases with ionizable surfactants. Moreover, with high concentration of reactants to trigger interfacial chemical reaction, spontaneous confined nanoemulsification can be achieved to produce much smaller sub-10-nm NEs (or called as swollen micelles) (Fig. 3e) [38]. Typically, with DCM droplet containing 50 vol% oleic acid (OA) added into a 0.2 mol/L NaOH solution, chemical reaction can be triggered at the O/W interface. This interfacial reaction rapidly produces overpopulated NaOA molecules precipitated as a thick and stable barrier at the droplet surface for tight confinement of the droplet. Then the confined droplet splits into smaller ones from generation to generation, and finally produces uniform sub-10-nm NEs *via* such a spontaneous confined nanoemulsification.

2.4. Bubble-bursting method

Bursting of bubbles is a phenomenon widely occurred in nature, which involves destabilization of interfaces. Harvest of the energy from bubble bursting enables formation of nanoemulsion droplets from an oil/water system. This bubble bursting strategy allows rup-

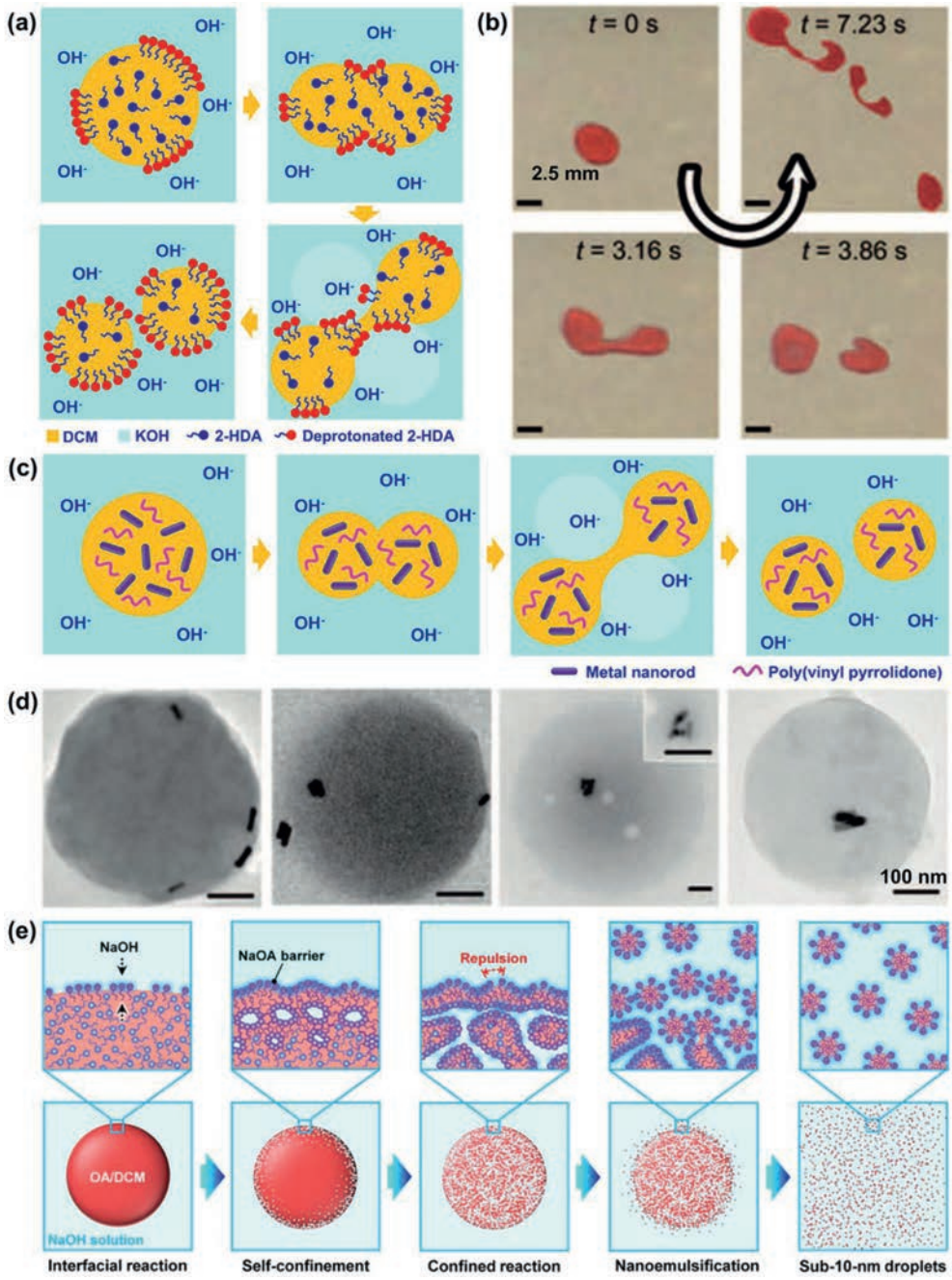

Fig. 3. Production of NEs *via* interfacial-reaction-induced droplet self-division. Illustration (a) and optical micrographs (b) of interfacial-reaction-induced spontaneous division of DCM/2-HDA droplets into smaller daughter droplets in KOH solution. (c) Illustration of formation of nanoemulsion droplets encapsulated with functional nanorods *via* droplet self-division. (d) TEM image of the resultant nanorod-containing nanodroplets. Reproduced with permission [34]. Copyright 2010, Wiley-VCH. (e) Schematics of spontaneous confined nanoemulsification process for creating sub-10-nm uniform nanoemulsion droplets. Reproduced with permission [38]. Copyright 2023, Wiley-VCH.

ture of an oil layer on top of the water phase to drive mass transfer from the upper oil phase to the lower water phase (Fig. 4a). The mass transfer then enables formation of nanoemulsion droplets with sizes of 100–800 nm and a moderate polydispersity index [39,40]. In a typical bubble bursting process (Fig. 4a), air bubbles are generated under a surfactant-containing water phase [39]. The water phase contains hexadecyltrimethylammonium bromide as surfactant and a thin oil layer of hexadecane on its top surface to create an air/oil/water interface for bubble bursting. As illustrated in Fig. 4b, when the bubble floats towards the air/oil/water interface, a bubble cap consisting of a water film and an oil film forms at the liquid surface. Due to the gravity and surface tension, the water and oil in the extruded film drain out, resulting in first rupture of the oil film and then the water film (Figs. 4b and c). The rupture and retraction of the water film eject a spray of oil nanodroplets from the cavity boundary into the bulk water phase (Figs. 4b and d). During the bubble bursting process, the size of generated droplet is controlled by the molecular-level interaction between oil molecules and the surfactants, and independent of hydrodynamics [39,40]. Moreover, by simply adding functional nanomaterials in the oil phase, the bubble-bursting system can produce functional nanoemulsion droplets encapsulated with these nanomaterials such as quantum dots (Figs. 4e–g) and silica NPs. For example, by dispersing green quantum dots (QDs) of cadmium selenide into the hexadecane layer with thickness of 1 mm, oil nanodroplets containing the green QDs, with mean droplet

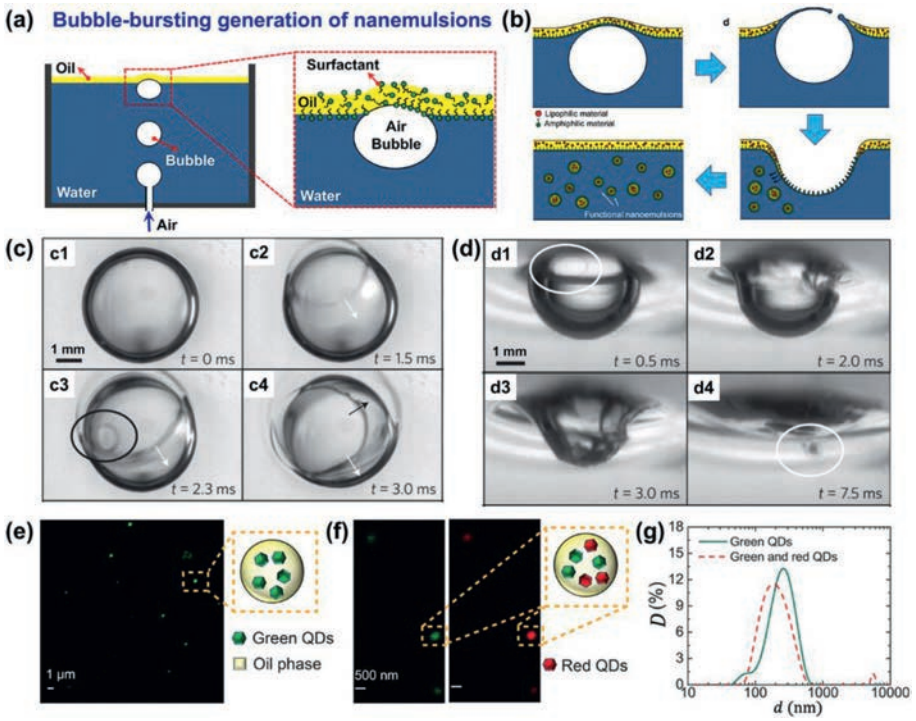

Fig. 4. Production of NEs *via* bubble bursting. Illustration showing generation of floating bubbles under surfactant-containing water with a top oil layer (a) for bubble bursting (b). Reproduced with permission [39]. Copyright 2016, Wiley-VCH. High-speed snapshots showing a bubble bursting at air/oil (c) and oil/water (d) interfaces. Reproduced with permission [40]. Copyright 2014, Springer Nature. NEs containing green QDs (e), and green and red QDs (f), and their size distributions (g). Reproduced with permission [39]. Copyright 2016, Wiley-VCH.

diameter of 214 nm and polydisperse index (PDI) of 0.374 can be produced after bubble bursting for 48 h (Figs. 4e and g). Moreover, with two different QDs (red and green) dispersed into the oil layer, oil nanodroplets containing both QDs, with mean droplet diameter of 232 nm and PDI of 0.258 can be produced (Figs. 4f and g). The bubble bursting method is applicable to liquid systems even with interfacial tension on the order of tens of mN/m, and shows no negative thermal effects as compared to the high-energy methods such as ultrasonication and high-pressure homogenization.

2.5. Micro-/nano-fluidic emulsification methods

Microfluidic techniques allow flexible and accurate manipulation of the flow and dispersion behaviors of multiple microflows in microchannel networks, thus showing great power in controllable generation of emulsion droplets [41–44]. Up to now, microfluidic devices with geometries such as co-flow, flow-focusing, and T-junction [45], are created from a variety of materials such as polydimethylsiloxane (PDMS), glass-capillary/plate [45–47], silicon [48], and polymethylmethacrylate [49]. These microfluidic devices enable controllable production of emulsion droplets from single emulsion droplets to higher-order multiple emulsion droplets [50–52]. The size of droplets from microfluidic techniques can be flexibly and precisely adjusted by tuning parameters such as the flow rate of dispersed and continuous phases and microchannel size. However, because the sizes of generated emulsion droplets from microfluidics largely depend on the minimum feature size of the microchannel, the minimum achievable sizes of these emulsion droplets are usually limited to a few micrometers. Although breakup of liquid threads by surface instability can produce satellite droplets with nanometer sizes [53], passive collection of these nanodroplets still suffers from low efficiency for nanoemulsion production because most volume of the liquid phase is used for microdroplet generation.

To directly and efficiently produce NEs, strategies based on electrostatic/hydrodynamic liquid-jet focusing [54], and supersonic microfluidic spray-drying [55,56], are developed. Typically, focusing a liquid flow can lead to capillary jetting at extremely small scale length to benefit the formation of nanoscale droplets. With strong shear stress from the continuous phase to focus the dispersed flow, surfactants can be accumulated at the tip of the dispersed flow to achieve a nearly zero surface tension for formation of a Taylor cone. From such a Taylor cone, a highly sharpened tip can be generated and broken up into tiny droplets with size in the nanometer scale. For continuous production of uniform NEs from a Taylor cone, a three-dimensional (3D) flow-focusing PDMS microfluidic device with a square waveform geometry (Fig. 5a) is developed [57]. In the flow-focusing junction, the dispersed water flow is sheared by the continuous mineral oil phase in all directions to form a symmetric conical liquid tip (Fig. 5b). Such a 3D flow-focusing device allows reduced energy and pressure for droplet breakup as compared to the 2D flow-focusing devices, thus enables generation of smaller droplets under certain operation pressures. In such a device, the droplet size can be flexibly manipulated from the micrometer scale to nanometer scale by adjusting the pressure ratio of water flow (P_w) to the mineral oil flow (P_o). As typically demonstrated in Fig. 5c, with the pressure ratio of $3.15/3.5 = 0.9$, microdroplets are generated in the dripping mode. When further decreasing the pressure ratio to $3.15/3.5 = 0.87$, the focused dispersed phase transits from the dripping mode into a tip-streaming mode, and forms a very thin liquid thread to produce W/O nanoemulsion droplets with a narrow size distribution (Fig. 5d). Moreover, besides the hydrodynamic strategy, the droplet breakup from a Taylor cone can also be enhanced by using electric field to produce nanoemulsion droplets [54,58,59]. Under such conditions, the nanodroplet size can be manipulated by adjusting the flow rates as well as the voltage of the electric field [58].

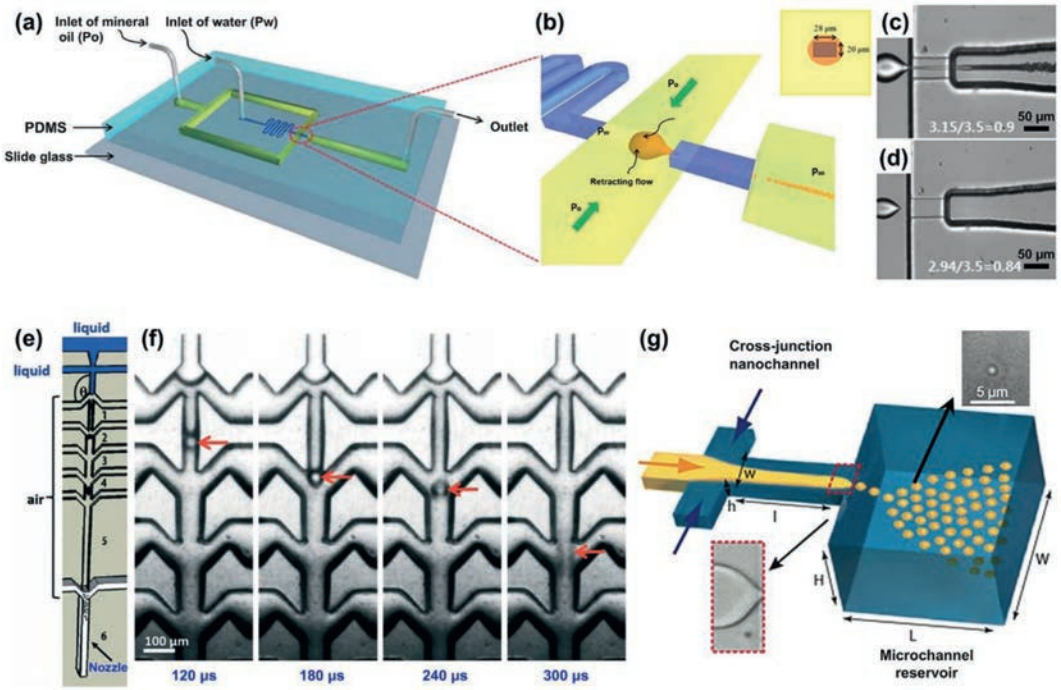

Fig. 5. Micro-/nano-fluidic techniques for controllable production of NEs. Illustration of microfluidic device (a) for continuous production of uniform NEs in a tip-streaming mode (b). High-speed snapshots of droplet breakup in dripping (c) and tip-streaming (d) mode with different pressure ratios. Reproduced with permission [57]. Copyright 2012, Royal Society of Chemistry. Illustration of the supersonic microfluidic spray-drying device (e) and time-lapse high-speed snapshots showing the droplet breakup in the device (f). Reproduced with permission [55]. Copyright 2017, Royal Society of Chemistry. (g) Illustration of micro-/nano-fluidic device with cross-junction nanochannel and microchannel reservoir for controllable production of NEs. Reproduced with permission [60]. Copyright 2010, American Chemical Society.

The formation of nanodroplets in microchannel usually requires significant enhancement of the shear stress for droplet breakup. Use of a supersonic air flow in microfluidic spray-drying devices provides an alternative and efficient way to achieve such enhancement of shear stress [55,56]. Fig. 5e shows the PDMS microfluidic device for the supersonic spray-drying [55]. The microfluidic device possesses two inlet microchannels at the top for injecting the dispersed liquid phase, and multiple pairs of inlet microchannels downstream for injecting the continuous air flow. During the microfluidic supersonic spray-drying process, the dispersed liquid phase is first dispersed by the air flow in the dripping regime to form primary microdroplets in air (Fig. 5f). Then, these microdroplets are sheared by supersonic air flow with high shear stress to form a large amount of much smaller daughter nanodroplets. By successively injecting air through the multiple air inlets into the main microchannel, the air flow can achieve a very high velocity and provide high shear stress to deform the generated droplets at each junction (Fig. 5f). This can produce airborne nanodroplets with size determined by the balance between the shear stress and Laplace pressure, which is much smaller than the microchannel dimension.

Since the droplet size is largely dependent on the size of flow channel, by reducing the channel dimension into nanometer size range, NEs can be produced [60,61]. As typically shown in Fig. 5g, the PDMS micro-/nano-fluidic device contains U-turn microchannels and a nanofluidic section with a cross junction and a terrace for nanoemulsion production [60]. The dispersed and continuous liquid phases that flow in the U-turn microchannels are driven into the cross-junction nanochannels. Sheared by the continuous phase, a jet stream from the dispersed phase is generated in the nanochannel, which then flows into the microchannel reservoir downstream. At the step between the nanochannel and microchannel reservoir, the capillary pressure difference dominates the droplet formation, leading to break-up of the jet stream into nanodroplets due to capillary instability [60,61]. Such a nanofluidic device allows generation of nanodroplets with high monodispersity (<5%) and high frequency (up to 15 kHz). Moreover, by varying the nanochannel height as well as the capillary pressure difference, nanodroplets with sizes in the range of 500∼1000 nm can be produced. These micro-/nano-fluidic techniques provide an efficient strategy for production of NEs with controllable size and high monodispersity.

3. Pharmaceutical delivery applications of nanoemulsions

NEs are powerful nanocarriers for pharmaceutical delivery, due to their features such as high surface area, high encapsulation efficiency, and improved thermodynamic stability. For the pharmaceutical delivery applications, high-energy emulsification such as ultrasonication, are commonly used to create NEs [62–65]. Recently, the low-energy emulsification has emerged as a promising way to create NEs for their applications due to some of their unique advantages as compared to the high-energy ones. For example, the low-energy methods consume less energy and their spontaneous formation of NEs simplifies the production process [5,66,67]. Meanwhile, the low-energy methods provide mild processes with reduced mechanical and thermal damage to labile active ingredients such as proteins. Moreover, the low-energy methods produce nanodroplets with smaller sizes and better size uniformity [38,39,57], that are difficult to achieve using the high-energy ones. This feature benefits the controllable nanoencapsulation in the NEs and predictable drug release profile, and creation of uniform and ultrasmall NPs carriers. Thus, here we highlight the use of NEs from the low-energy methods for pharmaceutical delivery applications, including their direct use as nanocarriers, and their use as templates to create functional NPs and NEs-incorporated or NPs-incorporated particles for pharmaceutical delivery.

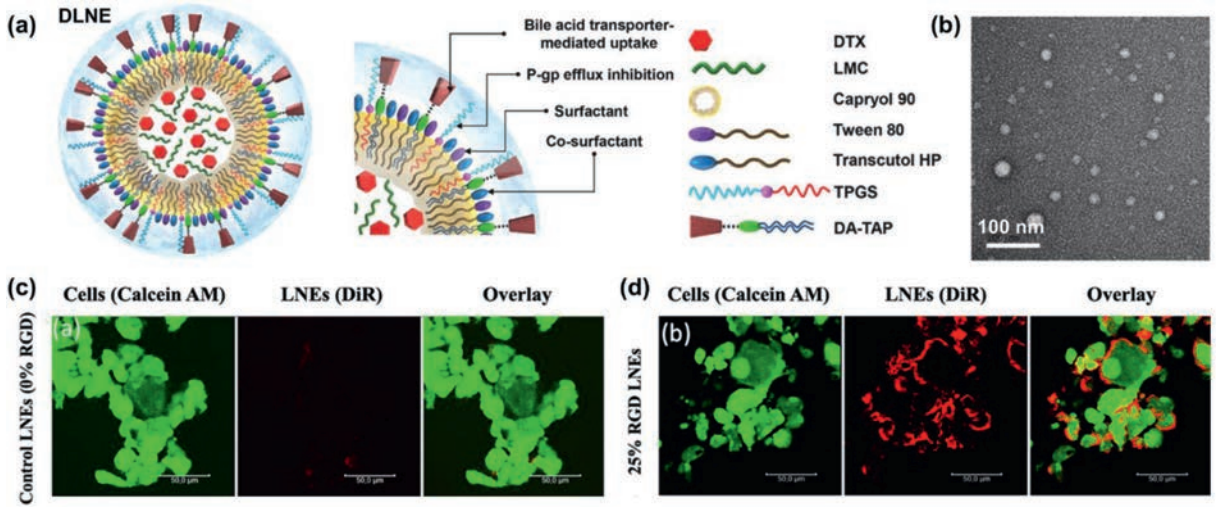

Fig. 6. NEs for advanced drug delivery. Illustration (a) and TEM image (b) of LMC/DTX loaded O/W NEs incorporating TPGS and an ionic complex of sodium deoxycholate and 1,2-dioleyl-3-trimethylammonium propane (DA-TAP). Reproduced with permission [80]. Copyright 2020, Elsevier. CLSM images of cellular uptake of unmodified (c) and 25 wt% RGD-modified (red) (d) lipid NEs after incubated with U-87 MG cells (green) for 1 h. Reproduced with permission [81]. Copyright 2020, American Chemical Society.

3.1. Nanoemulsions for pharmaceutical delivery

NEs provide advanced nano-platform for drug delivery in biomedical field [68–77]. Their oil and water phases create vast opportunities for flexibly loading both hydrophobic and hydrophilic pharmaceuticals [78]. Especially, the O/W NEs play a vital role for delivery of hydrophobic drugs, which are ubiquitous in a wide variety of applications including the pharmaceutical manufacturing. The drugs with poor water solubility show low-efficient penetration into the target tissues and organs, leading to poor bioavailability and absorption efficiency. The oil nanodroplets served as nanoreservoirs, can encapsulate these hydrophobic drugs with high capacity, protect them against hydrolysis and oxidation, and achieve efficient permeation across the barriers of biological membranes to improve drug bioavailability. For example, essential oil contains compounds that are beneficial to the defense response of plants either by direct antimicrobial activity against pathogens or repelling off insects, but the poor water-solubility of essential oil restricts its use in plants [5]. By modulating the viscosity of liquid phases for isothermal spontaneous emulsification under mild conditions, NEs of essential oil from cinnamon, clove, coriander, and red thyme are created [5]. To achieve stable essential oil NEs, soybean oil and propylene glycol are respectively used to tune the viscosity of organic and water phases, and Tween 80 is used as a surfactant. Such a spontaneous process largely simplifies the formulation and fabrication process, and efficiently produces essential oil NEs for pharmaceutical delivery in plants. In a plant-pathogen system (*A. thaliana-B. cinereal*), plants treated with the essential oil NEs show enhanced quantitative disease resistance (QDR) against the broad host-range necrotrophic phathogens (BHNs), due to enhanced production of jasmonic acid, upregulation of autophagy and ROS scavenging detoxification [5].

Docetaxel (DTX) is a semisynthetic paclitaxel derivative with excellent antitumor efficacy but still suffers from poor water-solubility [79]. Incorporation of methylcellulose (MLC)-complexed DTX in O/W NEs allows efficient oral delivery of DTX with enhanced absorption and anticancer efficacy for metronomic chemotherapy (Figs. 6a and b) [80]. Such O/W NEs are produced *via* low-energy spontaneous emulsification based on their *pseudo*-ternary phase diagram. These DTX-loaded O/W NEs, functionalized with D-alpha-tocopherol polyethylene glycol succinate (TPGS) for suppressing P-gp-mediated efflux and ion-pair complex for enhanced permeation, allow 249% increase in oral bioavailability as compared to free DTX.

Besides use of oil nanodroplets to enhance the bioavailability of poor water-soluble drugs, tailoring the surface property of nanodroplets provides another efficient way to benefit their improved interaction with the biological systems for better efficacy [63]. Typically, lipid NEs covalently grafted with high density of RGD peptide for surface modification are developed *via* a low-energy spontaneous emulsification technique [81]. As shown in Fig. 6c, after incubated with glioblastoma cells (U-87 MG cells) for 1 h, the RGD-modified lipid NEs are efficiently up-taken by the U-87 MG cells due to the ligand/receptor binding mechanism. However, without the RGD modification, the uptake of unmodified lipids NEs by the U-87 MG cells is very low (Fig. 6d). Moreover, when incubated with RAW 264.7 macrophages as the nontumorigenic cells, both the unmodified and RGD-modified lipid NEs exhibit almost no uptake by the macrophages, indicating their ability to address the undesired macrophage uptake in nanoparticulate-carrier-based therapy.

The nanoscale size and fluidic nature of NEs benefit their incorporation into larger scale materials such as milliparticles and films for their more flexible and efficient uses as delivery systems [65,82,83]. Such nanoemulsion-incorporated materials allow more efficient loading of poor water-soluble pharmaceuticals and more flexible and tunable release profiles, as compared to their counterparts without the NEs. For example, by incorporating ibuprofen-loaded NEs into millicapsules, drug release with three different release stages can be achieved [83]. NEs with oil droplets (~58 nm) of isopropyl myristate for loading the poor water-soluble ibuprofen (0.021 mg/mL at 25 °C) are created by using water phase containing sucrose and Ca^{2+} as continuous phase *via* a low-energy nanoemulsification process. When further dripping droplets of the NEs into aqueous alginate solution, millicapsules containing an alginate shell with mesh size of ~10 nm for efficient entrapment of the oil nanodroplets can be created *via* interfacial crosslinking (Fig. 7a). The capsule size and shell thickness can be flexibly tuned by changing the concentration of Ca^{2+} (Figs. 7b and c) and size of dispensing tip. The millicapsules in saline solution can achieve three-stage release behaviors of the loaded NEs (Fig. 7d). First, diffusion-based sustained release of the nanoemulsion cargo from the millicapsules are achieved due to the enlarged mesh size upon swelling of alginate shell in saline solution. Then the millicapsules enable

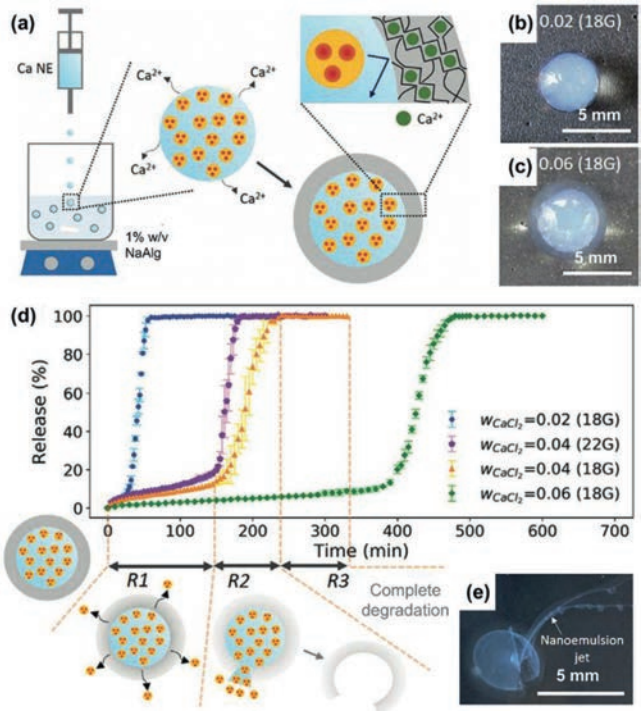

Fig. 7. NEs-incorporated milliparticles for controlled drug release. Illustration of dripping-based formation of alginate millicapsules containing ibuprofen-loaded NEs (a), with controlled capsule size and shell thickness (b, c). Release of ibuprofen from NEs-incorporated millicapsules (d) *via* diffusion-based sustained release (R1), burst release (R2) (e), and final post-release (R3). Reproduced with permission [83]. Copyright 2020, Wiley-VCH.

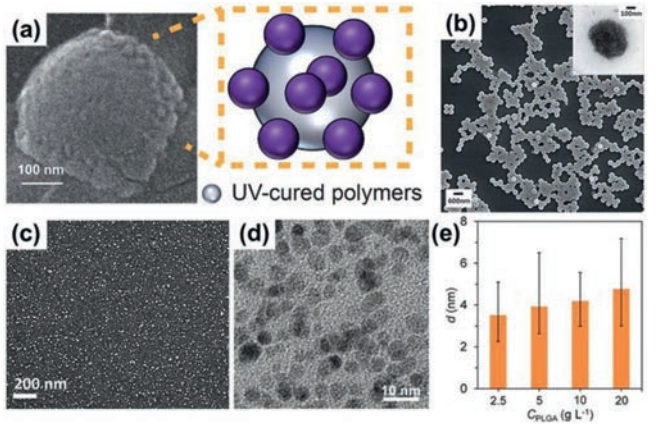

Fig. 8. Functional NPs created from nanoemulsion templates. (a) SEM image of a NOA89 nanoparticle decorated with silica NPs, using nanodroplets from bubble-bursting. Reproduced with permission [39]. Copyright 2016, Wiley-VCH. (b) SEM image of PEGDA NPs and TEM image of magnetic PEGDA NPs (inset) prepared using nanodroplets from microfluidic flow-focusing. Reproduced with permission [57]. Copyright 2012, Royal Society of Chemistry. (c) SEM image of $CaCO_3$ NPs prepared using nanodroplets from supersonic microfluidic spray-drying. Reproduced with permission [55]. Copyright 2017, Royal Society of Chemistry. TEM image of PLGA NPs (d) fabricated using spontaneous confined nanoemulsification, and their change of size (e) dependent on PLGA concentration. Reproduced with permission [38]. Copyright 2023, Wiley-VCH.

burst release of the nanoemulsion cargo (Fig. 7e) due to complete dissolution of alginate shell in the saline solution, followed with the final post-release of the cargo. The delayed time to achieve the burst-release stage can be easily controlled by tuning the shell thickness *via* adjustment of Ca^{2+} concentration during the millicapsule synthesis.

3.2. Nanoemulsion-derived nanoparticles for pharmaceutical delivery

Functional NPs are broadly used in myriad fields such as catalytic and biomedical fields. In biomedical field, NPs show great power as delivery systems of pharmaceuticals, due to their distinct properties as compared to individual molecules and larger sized particles [84–90]. Generally, the size and surface property of NPs greatly affect their behaviors in biological systems after administration, such as their circulation time, clearance, and biodistribution [12,91–93]. For example, hydrophilic NPs with sizes of 10∼100 nm can escape from phagocytosis of the reticuloendothelial system, and allow a longer circulation time in blood vessels [94,95]. NPs with sizes less than 10 nm usually show efficient permeability across the blood–brain barrier with pore size upper limit of ∼12 nm for treatment of central nervous system diseases, while the larger ones are mostly hampered [94,96,97]. Moreover, NPs with sizes less than 5.5 nm can be rapidly cleared from the blood *via* renal clearance, which benefits their complete elimination from human body [91,94,98]. Thus, controlling the features of NPs such as their size and physicochemical properties plays key roles in determining their performance as pharmaceutical delivery systems in biomedical field.

Generally, NPs can be produced *via* methods such as emulsion polymerization, suspension polymerization, ball-milling, nanocrystallization, nanoprecipitation, and template synthesis from nanodroplets [99–102]. Among these methods, NEs with nanoscale droplets of water or oil provide powerful templates for synthesizing functional NPs with size and composition similar to those of the nanodroplets [13,39,56,57,62,103–106]. Meanwhile, the flexible compositions in the dispersed nanodroplets and continuous phase, and at their interfaces, provide versatile opportunities to engineer the composition, structure and function of the interior and surface of the NPs. Usually, NPs are created using NEs produced from methods such as the ultrasonication, high-pressure homogenization and high-shear mixing. However, due to the polydisperse nanoemulsion templates, the resultant NPs are usually non-uniform. Uniform NEs from low-energy methods such as bubble-bursting and micro-/nano-fluidic emulsification provide new opportunities to create NPs with improved uniformity [39,57,107]. For example, by using hexadecane containing UV-curable polymers NOA89 as the oil phase and silica NPs as the emulsifier, nanodroplets with the silica NPs stabilized at the surface can be produced *via* the bubble bursting process [39]. UV-polymerization of such nanodroplets can create polymeric NPs with silica NPs decorated on their surface (Fig. 8a). These NOA89 NPs show improved uniformity due to the moderate PDI of nanodroplet templates from bubble bursting [39]. Moreover, more uniform NPs can be created by using monodisperse nanodroplets from micro-/nano-fluidic emulsification [55,57]. By simply adding polyethylene glycol diacrylate (PEGDA) and photo-initiator in the water phase to produce nanodroplets using the flow-focusing microfluidic device (Fig. 5a), uniform PEGDA NPs can be continuously created by fast UV-induced polymerization [57]. The PEGDA NPs show an average size of ∼360 nm, and CV value of 3.38%, indicating their sizes are highly monodisperse (Fig. 8b). Further incorporation of magnetic iron oxide NPs in PEGDA-containing water phase for the microfluidic nanoemulsification allows production of PEGDA NPs with embedded magnetic cores (inset in Fig. 8b).

Usually, as compared to their nanoemulsion templates, the obtained NPs show reduced sizes due to the volume shrinkage in the liquid-to-solid conversion. Thus, with further reduce of the nanodroplet size, ultrasmall functional NPs can be produced. For example, with high shear stress from supersonic microfluidic spray-drying to produce smaller nanodroplets, uniform amorphous $CaCO_3$ NPs with an average diameter of 12 nm can be created

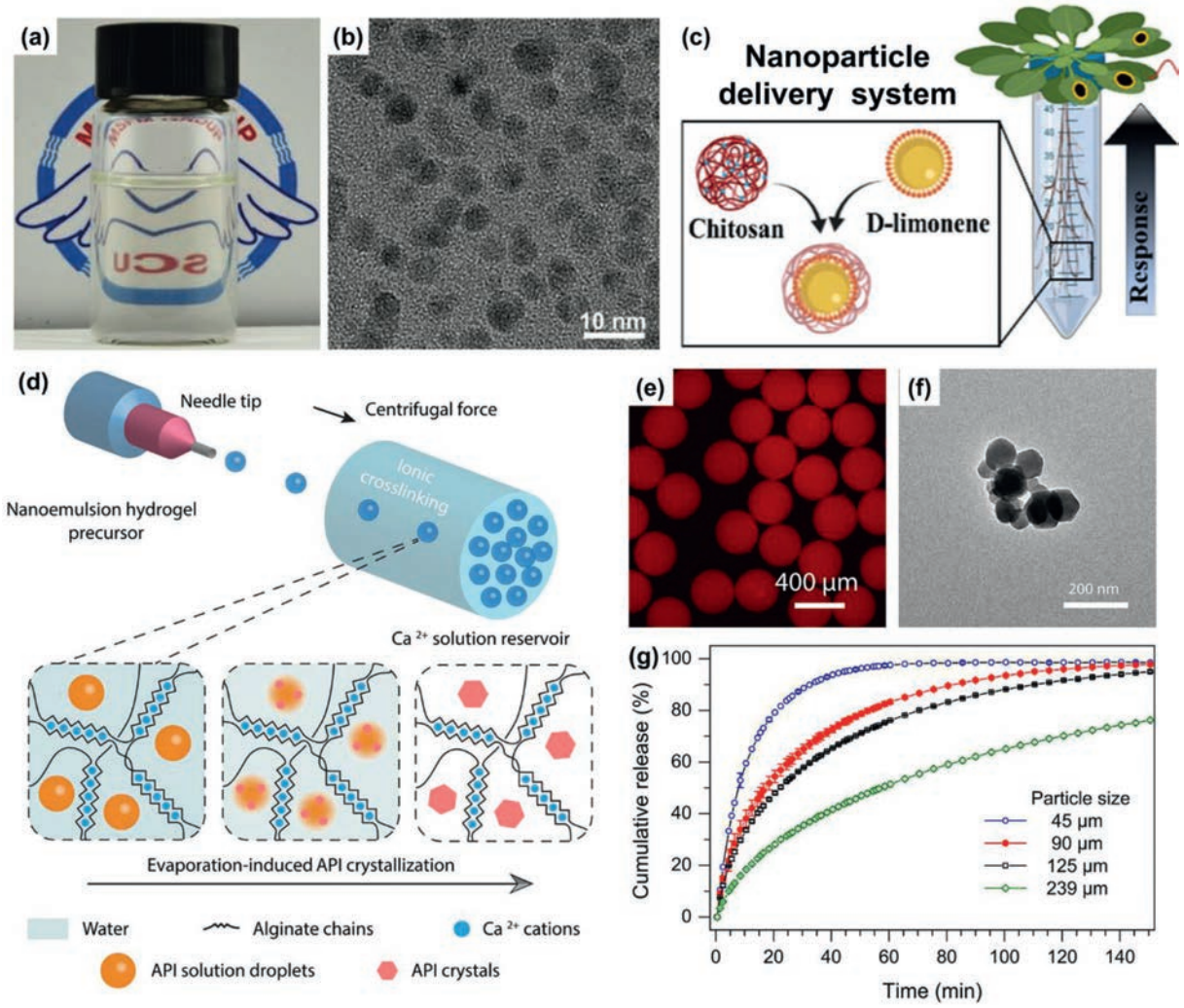

Fig. 9. Functional NPs from NEs for biomedical application. Photo of an aqueous solution containing sub-10-nm CPT-loaded PLGA NPs (a) and TEM image of these NPs (b). Reproduced with permission [38]. Copyright 2023, Wiley-VCH. (c) Chitosan NPs loaded with D-limonene nanodroplets for enhancing the QDR of plants against BHNs. Reproduced with permission [111]. Copyright 2021, American Chemical Society. (d) Synthesis of fenofibrate-nanoparticle-loaded alginate microparticles using nanoemulsion-loaded droplets as templates, *via* Ca^{2+}-crosslinking and evaporation-induced nanocrystallization. (e) Fluorescent micrograph of microgel particles with NEs containing Nile-red-dyed fenofibrate. (f) TEM image of the recovered fenofibrate nanocrystals from the dried microgel particles with 70.7% drug loads. (g) Cumulative release profiles of the dried microgel particles with 70.7% drug loads and different sizes. Reproduced with permission [112]. Copyright 2020, American Chemical Society.

(Fig. 8c) [56]. Moreover, the tiny nanodroplets from supersonic microfluidic spray-drying even enable production of ultrasmall NPs of amorphous NaCl which usually shows a very high propensity to crystallize [56]. Besides, the sub-10-nm NEs from spontaneous confined nanoemulsification provide excellent templates to create ultrasmall NPs. With sub-10-nm NEs droplets containing biocompatible poly(lactic-*co*-glycolic acid) (PLGA) from spontaneous confined nanoemulsification as templates, uniform and ultrasmall PLGA NPs can be produced *via* further solvent evaporation of DCM in the NEs (Fig. 8d) [38]. Regulation of the PLGA concentration in the nanodroplets from 20 g/L to 2.5 g/L allows decreasing the size of PLGA NPs from ~4.8 nm to ~3.5 nm (Fig. 8e). The NPs with ultrasmall sub-10-nm sizes may find promising uses for pharmaceutical delivery since they usually enable increased tumor penetration, more precise tumor targeting and effective cancer therapy as compared to the larger ones [108].

The flexible control of composition and size of NEs provides vast opportunities to create drug-loaded functional NPs for pharmaceutical delivery. The NEs allow first loading of drug molecules in their nanodroplets during the nanoemulsification process, and then creation of drug-loaded NPs *via* physical/chemical processes such as temperature-induced phase change and interfacial crosslinking [109,110]. Such a strategy benefits efficient preloading of desired drugs in the resultant NPs to achieve advanced delivery of the drugs with improved bioavailability. For example, camptothecin (CPT), an anticancer drug with good antineoplastic activity against brain, lung and breast tumors, can be loaded into NPs *via* the spontaneous confined nanoemulsification [38]. By dissolving CPT in a PLGA-containing OA/DCM phase, NEs with sub-10-nm oil nanodroplets containing PLGA and CPT can be created *via* the spontaneous confined nanoemulsification. Further evaporation of the DCM in the NEs produces homogeneous dispersion of CPT-loaded PLGA nanoparticles with size of sub-10 nm (Figs. 9a and b). Besides, drug-loaded NPs with core-shell structures can be developed using nanoemulsion droplets as templates. For instance, with the D-limonene NEs made from isothermal spontaneous emulsification as templates, NPs with a chitosan shell and an essential oil core (D-limonene) are developed *via* ionic gelation (Fig. 9c) [111]. With the chitosan as an elicitor of the plant immune system, and antimicrobial essential oil as activator of the plant defense response, such core-shell NPs can trigger an on-demand systemic defense response in plants to achieve enhanced QDR against BHNs in the *A. thaliana-B. cinerea* model system.

Table 1
Summary of typical low-energy nanoemulsification methods.

Method	NEs type	Typical droplet size	Typical composition of O and W phases	Advantages (A) & disadvantages (D)	Application	Ref.
Vapor condensation	W/O	~430 nm - ~200 nm	O: dodecane and Span 80 W: water vapor	A: simple production process D: high surfactant content, droplet size of ~10% PDI, difficult to encapsulate contents	/	[28]
Vapor condensation	W/O	~500 nm - ~100 nm	O: dodecane, kerosene, and silica NPs W: water vapor	A: simple production process D: relatively broad size distribution, difficult to encapsulate contents	/	[30]
Cycled cooling-heating	O/W	~1200 nm - ~600 nm	O: linear alkanes with chain length varying from C_{14} (tetradecane) to C_{20} (eicosane) W: water and surfactant (cetyltrimethylammonium bromide or sodium octadecyl sulfate)	A: relatively simple production process D: relatively large droplet size and repeated temperature control	/	[21]
Self-division	O/W	~350 nm - ~30 nm	O: DCM and 2-HDA W: KOH solution	A: simple production process, uniform droplet size D: limited choices of encapsulation contents due to high pH, high surfactant content	Nano-encapsulation	[34]
Self-division	O/W	~650 nm - <10 nm	O: DCM and OA W: NaOH solution	A: simple production process, uniform and ultrasmall droplet size D: limited choices of encapsulation contents due to high pH, high surfactant content	Drug-loaded NPs synthesis	[38]
Bubble-bursting	O/W	~230 nm - ~100 nm	O: *n*-hexadecane, *n*-pentadecane, *n*-tetradecane, *n*-tridecane, *n*-dodecane, *n*-undecane, *n*-decane, PDMS or NOA 89 W: water and sufactants (hexadecyltrimethylammonium bromide, dodecyltrimethylammonium bromide, docusate sodium, or sodium dodecyl sulphate)	A: simple production process D: limited volume of dispersed phase and droplet size with moderate PDI	NPs synthesis	[40]
Bubble-bursting	O/W	~800 nm - ~100 nm	O: *n*-hexadecane, *n*-tridecane, and *n*-hexane W: water and hexadecyltrimethylammonium bromide	A: simple production process D: limited volume of dispersed phase and droplet size with moderate PDI	Nano-encapsulation and NPs synthesis	[39]
Microfluidic flow-focusing	W/O	~5 μm - ~400 nm	O: Mineral oil and surfactant ABIL EM90 W: water	A: highly controllable and monodisperse droplet size D: complex device construction and troublesome flow manipulation	NPs synthesis	[57]
Nanofluidic capillary-focusing	O/W	~4 μm - ~900 nm	O: fluorinated oil W: water and sodium dodecyl sulfate	A: uniform droplet size D: complex device construction, troublesome flow manipulation and relatively large droplet size	Particle synthesis	[60]

Incorporation of NPs into larger scale materials such as microparticles provides more flexibility for the composite materials to achieve versatile drug release [62]. Usually, by using NEs-loaded micro-/milli-droplets as templates, NPs-loaded micro-/milli-particles can be developed by respectively solidifying the nanoemulsion droplets and micro-/milli-droplets [62,112]. For instance, alginate microparticles loaded with fenofibrate NPs are created *via* a scalable, low-energy process, using NEs-loaded microdroplets as templates to achieve high loading capacity and fast release of fenofibrate (Fig. 9d). First, O/W NEs are prepared *via* spontaneous emulsification, using fenofibrate-containing anisole as dispersed phase and alginate solution with surfactants Span 80 and Tween 80 as continuous phase. Further dispersion of the NEs into microdroplets, followed with Ca^{2+} crosslinking of the microdroplets and evaporation-induced nanocrystallization of fenofibrate in the NEs droplets, produces alginate microparticles (Fig. 9e) loaded with fenofibrate NPs (Fig. 9f). Fenofibrate is a highly hydrophobic drug that typically used to treat high blood lipoprotein concentrations *via* oral administration, but usually suffers from very poor water-solubility (<1 μg/mL). This low-energy nanoemulsification with optimized surfactant amount enables high load of drugs (>70%) in the resultant alginate microparticles. The drug release kinetics of the fenofibrate-NPs-loaded microparticles can be modulated by adjusting the drug load and microparticle size. Typically, decrease of the microparticle size from 239 μm to 45 μm can lead to a highly accelerated release rate (Fig. 9g), showing a significant dissolution enhancement (up to 70×) compared to bulk fenofibrate crystals. Such NPs-loaded microparticles are promising as advanced drug delivery systems with both high drug load and fast drug release for hydrophobic compounds.

4. Conclusions

This review provides a summary on the recent development of low-energy nanoemulsification techniques for creating NEs, and the use of NEs and NEs-derived particles for advanced pharmaceutical delivery in biomedical fields. Low-energy nanoemulsification techniques that employ elaborate interfacial science and micro-/nano-fluidics to produce controllable NEs, are introduced (typical low-energy nanoemulsification methods introduced in this review are summarized in Table 1). Then, use of NEs as pharmaceutical delivery systems for biomedical application is introduced, with highlights on the NEs loaded with poor water-soluble drugs. Meanwhile, the NEs provide encapsulated drug nanocarriers to create NEs-incorporated milli-particles and offer advanced templates to create functional NPs with sizes down to sub-10 nm, and NPs-incorporated microparticles. The NEs and their derived particles, with well-designed sizes and compositions, provide advanced pharmaceutical delivery systems with improved drug bioavailability and efficacy for treatment of diseases. Future efforts should focus on developing more robust nanoemulsification equipments and new low-energy nanoemulsification methods, and exploring their possible combinations to achieve controllable, continuous and scalable production of NEs. Moreover, deep insights into the relationship between the features of surfactants/combined surfactants and their interfacial assembly behaviors are required, since their assembly behaviors largely determine the size and structure of NEs. The revealed interfacial science may guide the rational molecular design of surfactants for controllable formation of NEs, especially those with multiple-layered interiors, *via* a surfactant-assembly guided process. Such advances will promote the rational design and production of desired NEs and NEs-derived NPs for pharmaceutical delivery application in biomedical field.

Declaration of competing interest

The authors declare that they have no known competing financial interests or personal relationships that could have appeared to influence the work reported in this paper.

Acknowledgments

The authors gratefully acknowledge support from the National Natural Science Foundation of China (Nos. 22108186, 21922809, 21991101), and Sichuan University (No. 2020SCUNG112).

References

[1] K. Li, Y. Zhao, J. Yang, J. Gu, Nat. Commun. 13 (2022) 1879.
[2] K. Sharma, A. Babaei, K. Oberoi, et al., Food Bioprocess Technol. 15 (2022) 2375–2395.
[3] R.M. Rodrigues, X. Guan, J.A. Iniguez, et al., Nat. Catal. 2 (2019) 407–414.
[4] S.M. Hashemnejad, A.M. Badruddoza, B. Zarket, C.R. Castaneda, P.S. Doyle, Nat. Commun. 10 (2019) 2749.
[5] P. Vega-Vásquez, N.S. Mosier, J. Irudayaraj, ACS Nano 15 (2021) 8338–8349.
[6] T. Sheth, S. Seshadri, T. Prileszky, M.E. Helgeson, Nat. Rev. Mater. 5 (2020) 214–228.
[7] T. Jiang, W. Liao, C. Charcosset, Food Res. Int. 132 (2020) 109035.
[8] H. Qin, H. Zhang, X. Zhou, et al., Chin. Chem. Lett. 31 (2020) 292–294.
[9] J. Yang, Z. Dong, W. Liu, et al., Chin. Chem. Lett. 31 (2020) 875–879.
[10] K. Luisi, K.M. Morabito, K.E. Burgomaster, et al., Sci. Adv. 6 (2020) 5068.
[11] M. Singh, S. Bharadwaj, K.E. Lee, S.G. Kang, J. Control. Release 328 (2020) 895–916.
[12] M.J. Mitchell, M.M. Billingsley, R.M. Haley, et al., Nat. Rev. Drug Discov. 20 (2021) 101–124.
[13] A. Elzayat, I. Adam-Cervera, O. Álvarez-Bermúdez, R. Muñoz-Espí, Colloids Surf. B 203 (2021) 111764.
[14] Y. Singh, J.G. Meher, K. Raval, et al., J. Control. Release 252 (2017) 28–49.
[15] A. Naseema, L. Kovooru, A.K. Behera, K.P.P. Kumar, P. Srivastava, Adv. Colloid Interface Sci. 287 (2021) 102318.
[16] T. Tadros, P. Izquierdo, J. Esquena, C. Solans, Adv. Colloid Interface Sci. 108-109 (2004) 303–318.
[17] C. Solans, D. Morales, M. Homs, Curr. Opin. Colloid Interface Sci. 22 (2016) 88–93.
[18] S.M.M. Modarres-Gheisari, R. Gavagsaz-Ghoachani, M. Malaki, P. Safarpour, M. Zandi, Ultrason. Sonochem. 52 (2019) 88–105.
[19] J.S. Komaiko, D.J. McClements, Compr. Rev. Food Sci. Food Saf. 15 (2016) 331–352.
[20] P. Chuesiang, U. Siripatrawan, R. Sanguandeekul, L. McLandsborough, D.J. McClements, J. Colloid Interface Sci. 514 (2018) 208–216.
[21] S. Tcholakova, Z. Valkova, D. Cholakova, et al., Nat. Commun. 8 (2017) 15012.
[22] A. Perazzo, V. Preziosi, S. Guido, Adv. Colloid Interface Sci. 222 (2015) 581–599.
[23] M.J. Zhang, W. Wang, X.L. Yang, et al., ACS Appl. Mater. Interfaces 7 (2015) 13758–13767.
[24] L. Chen, M.J. Zhang, S.Y. Zhang, et al., ACS Appl. Mater. Interfaces 12 (2020) 35120–35131.
[25] Y.Y. Su, M.J. Zhang, W. Wang, et al., Ind. Eng. Chem. Res. 58 (2019) 1590–1600.
[26] R. Xie, F. Luo, L. Zhang, et al., Small 14 (2018) 1703650.
[27] Y. Wang, Z. Liu, F. Luo, et al., J. Membr. Sci. 575 (2019) 28–37.
[28] I.F. Guha, S. Anand, K.K. Varanasi, Nat. Commun. 8 (2017) 1371.
[29] S. Anand, K. Rykaczewski, S.B. Subramanyam, D. Beysens, K.K. Varanasi, Soft Matter 11 (2015) 69–80.
[30] D.J. Kang, H. Barannia, S. Anand, ACS Appl. Mater. Interfaces 10 (2018) 21746–21754.
[31] B.P. Binks, Curr. Opin. Colloid Interface Sci. 7 (2002) 21–41.
[32] B. Wu, C. Yang, Q. Xin, et al., Adv. Mater. 33 (2021) 2102362.
[33] N. Denkov, S. Tcholakova, I. Lesov, D. Cholakova, S.K. Smoukov, Nature 528 (2015) 392–395.
[34] K.P. Browne, D.A. Walker, K.J.M. Bishop, B.A. Grzybowski, Angew. Chem. Int. Ed. 49 (2010) 6756–6759.
[35] A.Z. Patashinski, R. Orlik, K. Paclawski, M.A. Ratner, B.A. Grzybowski, Soft Matter 8 (2012) 1601–1608.
[36] F. Caschera, S. Rasmussen, M.M. Hanczyc, ChemPlusChem 78 (2013) 52–54.
[37] C. Almarcha, P.M.J. Trevelyan, P. Grosfils, A. De Wit, Phys. Rev. Lett. 104 (2010) 044501.
[38] C. Chen, Q.W. Cai, C.Z. Zhan, et al., Small 19 (2023) 2300801.
[39] J. Feng, J.K. Nunes, S. Shin, et al., Adv. Mater. 28 (2016) 4047–4052.
[40] J. Feng, M. Roché, D. Vigolo, et al., Nat. Phys. 10 (2014) 606–612.
[41] W. Wang, P.F. Li, R. Xie, et al., Adv. Mater. 34 (2022) 2107877.
[42] L. Cai, F. Bian, H. Chen, et al., Chem 7 (2021) 93–136.
[43] B. Wang, P. Prinsen, H. Wang, et al., Chem. Soc. Rev. 46 (2017) 855–914.
[44] Y. Zhao, M. Zhang, X. Wen, Z. Xiang, Green Chem. Eng. 1 (2020) 63–69.
[45] W. Wang, R. Xie, X.J. Ju, et al., Lab Chip 11 (2011) 1587–1592.
[46] Z.J. Meng, W. Wang, X. Liang, et al., Lab Chip 15 (2015) 1869–1878.
[47] N.N. Deng, Z.J. Meng, R. Xie, et al., Lab Chip 11 (2011) 3963–3969.
[48] S. Yadavali, H.H. Jeong, D. Lee, D. Issadore, Nat. Commun. 9 (2018) 1222.
[49] D. Conchouso, D. Castro, S.A. Khan, I.G. Foulds, Lab Chip 14 (2014) 3011–3020.
[50] W. Wang, M.J. Zhang, L.Y. Chu, Acc. Chem. Res. 47 (2014) 373–384.
[51] W. Li, L. Zhang, X. Ge, et al., Chem. Soc. Rev. 47 (2018) 5646–5683.
[52] L. Shang, Y. Cheng, Y. Zhao, Chem. Rev. 117 (2017) 7964–8040.
[53] Y.C. Tan, A.P. Lee, Lab Chip 5 (2005) 1178–1183.
[54] K.H. Roh, D.C. Martin, J. Lahann, Nat. Mater. 4 (2005) 759–763.
[55] E. Amstad, F. Spaepen, M.P. Brenner, D.A. Weitz, Lab Chip 17 (2017) 1475–1480.
[56] E. Amstad, M. Gopinadhan, C. Holtze, et al., Science 349 (2015) 956–960.
[57] W.C. Jeong, J.M. Lim, J.H. Choi, et al., Lab Chip 12 (2012) 1446–1453.
[58] H. Kim, D. Luo, D. Link, et al., Appl. Phys. Lett. 91 (2007) 133106.
[59] Á.G. Marín, I.G. Loscertales, M. Márquez, A. Barrero, Phys. Rev. Lett. 98 (2007) 014502.
[60] F. Malloggi, N. Pannacci, R. Attia, et al., Langmuir 26 (2010) 2369–2373.
[61] L. Shui, E. Stefan Kooij, D. Wijnperlé, A. van den Berg, J.C.T. Eijkel, Soft Matter 5 (2009) 2708–2712.
[62] X.L. Yang, X.J. Ju, X.T. Mu, et al., ACS Appl. Mater. Interfaces 8 (2016) 10524–10534.
[63] Y. Zhang, Y. Liao, Q. Tang, J. Lin, P. Huang, Angew. Chem. Int. Ed. 60 (2021) 10647–10653.
[64] X. Lin, Y. Sheng, X. Zhang, et al., J. Control. Release 346 (2022) 380–391.
[65] L.H. Chen, P.S. Doyle, Adv. Mater. 33 (2021) 2008618.
[66] H.F. Fritz, A.C. Ortiz, S.P. Velaga, J.O. Morales, Drug Deliv. Transl. Res. 8 (2018) 1807–1814.
[67] N. Patel, H. Nakrani, M. Raval, N. Sheth, Drug Deliv. 23 (2016) 3712–3723.
[68] A.S. Klymchenko, F. Liu, M. Collot, N. Anton, Adv. Healthc. Mater. 10 (2021) 2001289.
[69] N. Qiu, Y. Liu, Q. Liu, et al., Biomaterials 269 (2021) 120604.
[70] C. Liu, H. Lai, T. Chen, ACS Nano 14 (2020) 11067–11082.
[71] V.K. Rai, N. Mishra, K.S. Yadav, N.P. Yadav, J. Control. Release 270 (2018) 203–225.
[72] C. Gang, W. Kaikai, W. Pengkai, et al., Nano Res. 11 (2018) 3746–3761.
[73] F. Xia, W. Fan, S. Jiang, et al., ACS Appl. Mater. Interfaces 9 (2017) 21660–21672.
[74] X. Zhou, Y. Hao, L. Yuan, et al., Chin. Chem. Lett. 29 (2018) 1713–1724.
[75] D. Liu, B. Wan, J. Qi, et al., Chin. Chem. Lett. 29 (2018) 1834–1838.
[76] L.R. Michels, F.N.S. Fachel, R.S. Schuh, et al., J. Control. Release 355 (2023) 343–357.
[77] M. Nasr, Drug Deliv. 23 (2016) 1444–1452.
[78] N. Nagai, H. Otake, Adv. Drug Deliv. Rev. 191 (2022) 114582.
[79] R. Ghadi, N. Dand, J. Control. Release 248 (2017) 71–95.

[80] S.K. Jha, J.Y. Chung, R. Pangeni, et al., J. Control. Release 328 (2020) 368–394.
[81] M.F. Attia, M.I. Swasy, R. Akasov, F. Alexis, D.C. Whitehead, ACS Appl. Bio Mater. 3 (2020) 5067–5079.
[82] L.H. Chen, P.S. Doyle, Chem. Mater. 34 (2022) 5194–5205.
[83] L.H. Chen, L.C. Cheng, P.S. Doyle, Adv. Sci. 7 (2020) 2001677.
[84] W. Chen, L. Jiang, Y. Hu, et al., J. Control. Release 340 (2021) 342–360.
[85] H. Liu, Z. Miao, Z. Zha, Chin. Chem. Lett. 33 (2022) 1673–1680.
[86] S. Wang, Y. Zhao, Z. Zhang, Y. Zhang, L. Li, Chin. J. Chem. Eng. 38 (2021) 30–42.
[87] H. Liu, X.Y. Li, X. Li, J.D. Huang, Green Chem. Eng. 4 (2023) 399–416.
[88] J. Zhang, K. Hu, L. Di, et al., Adv. Drug Deliv. Rev. 178 (2021) 113964.
[89] S. Quader, K. Kataoka, H. Cabral, Adv. Drug Deliv. Rev. 182 (2022) 114115.
[90] T. Tian, J. Ruan, J. Zhang, et al., J. Biomed. Nanotechnol. 18 (2022) 660–676.
[91] W. Jiang, C.A. von Roemeling, Y.X. Chen, et al., Nat. Biomed. Eng. 1 (2017) 0029.
[92] H. Han, S. Li, M. Xu, et al., Adv. Drug Deliv. Rev. 196 (2023) 114770.
[93] M. Placci, M.I. Giannotti, S. Muro, Adv. Drug Deliv. Rev. 197 (2023) 114683.
[94] M. Elsabahy, K.L. Wooley, Chem. Soc. Rev. 41 (2012) 2545–2561.
[95] T.T. Zhang, W. Li, G.M. Meng, P. Wang, W.Z. Liao, Biomater. Sci. 4 (2016) 219–229.
[96] K. Hou, J. Zhao, H. Wang, et al., Nat. Commun. 11 (2020) 4790.
[97] T.G. Chan, S.V. Morse, M.J. Copping, J.J. Choi, R. Vilar, ChemMedChem 13 (2018) 1311–1314.
[98] C. Ghimire, H.Z. Wang, H. Li, et al., ACS Nano 14 (2020) 13180–13191.
[99] C.J. Martínez Rivas, M. Tarhini, W. Badri, et al., Int. J. Pharm. 532 (2017) 66–81.
[100] J.P. Rao, K.E. Geckeler, Prog. Polym. Sci. 36 (2011) 887–913.
[101] R. Ghosh Chaudhuri, S. Paria, Chem. Rev. 112 (2012) 2373–2433.
[102] C.I.C. Crucho, M.T. Barros, Mater. Sci. Eng. C 80 (2017) 771–784.
[103] B. Kupikowska-Stobba, M. Kasprzak, J. Mater. Chem. B 9 (2021) 5221–5244.
[104] S. Leitner, C. Solans, M.J. García-Celma, G. Calderó, Carbohydr. Polym. 205 (2019) 117–124.
[105] C. Fornaguera, N. Feiner-Gracia, G. Calderó, M.J. García-Celma, C. Solans Nanoscale 7 (2015) 12076–12084.
[106] L. Peng, C.T. Hung, S. Wang, et al., J. Am. Chem. Soc. 141 (2019) 7073–7080.
[107] C. Fornaguera, A. Dols-Perez, G. Calderó, et al., J. Control. Release 211 (2015) 134–143.
[108] G. Feng, J. Liu, R. Liu, et al., Adv. Sci. 4 (2017) 1600407.
[109] A. Nabawy, J.M. Makabenta, S. Schmidt-Malan, et al., J. Control. Release 347 (2022) 379–388.
[110] P.Y. Lin, K.H. Chen, Y.B. Miao, et al., Adv. Funct. Mater. 29 (2019) 1809015.
[111] P. Vega-Vásquez, N.S. Mosier, J. Irudayaraj, ACS Sustain. Chem. Eng. 9 (2021) 9903–9914.
[112] T. Domenech, P.S. Doyle, Chem. Mater. 32 (2020) 498–509.